



Synthesis of NiTi microtubes via the Kirkendall effect during interdiffusion of Ti-coated Ni wires[☆]



A.E. Paz y Puente^{a,*}, D.C. Dunand^b

^a Department of Mechanical and Materials Engineering, University of Cincinnati, 598 Rhodes Hall, P.O. Box 210072, Cincinnati, OH, 45221, USA

^b Department of Materials Science and Engineering, Northwestern University, 2220 Campus Drive, Evanston, IL, 60208, USA

ARTICLE INFO

Keywords:

NiTi
Pack cementation
Diffusion coatings
Kirkendall effect
Microtubes

ABSTRACT

An additive alloying method is developed to fabricate NiTi microtubes, consisting of two steps: (i) depositing a Ti-rich coating onto ductile, pure Ni wires (50 μm in diameter) via pack cementation, resulting in a Ni core coated with concentric NiTi₂, NiTi and Ni₃Ti shells, and (ii) homogenizing the coated wires to near equiatomic NiTi composition via interdiffusion between core and shells, while concomitantly creating Kirkendall pores. Because of the spatial confinement and radial symmetry of the interdiffusing core/shell structure, the Kirkendall pores coalesce near the center of the wire and form a continuous longitudinal channel, thus creating a microtube. To study the evolution of Ni-Ti phases and Kirkendall pores during homogenization, coated wires were subjected to *ex situ* homogenization followed by (i) metallography and (ii) X-ray tomographic imaging. Near equiatomic NiTi was obtained upon homogenization at 925 °C for 4 h with compositional fluctuations between 49 and 53 at. % Ni consistent with slight variations in initial coating thickness. Kirkendall pores initially formed near the NiTi/Ni₃Ti and Ni₃Ti/Ni interfaces and eventually merged into a continuous channel with an aspect ratio of at least 75.

1. Introduction

Near equiatomic NiTi has been widely studied because of its shape memory and superelastic behavior [1–6]. While bulk NiTi has a broad variety of actuation, damping and structural uses due to these properties, porous NiTi structures offer the additional benefits of having low density, low stiffness and high surface area, which provide advantages for light-weight actuation [7], damping [8], and biomedical applications [9–12]. In particular, open pores enable the flow of fluids for efficient heating and cooling, which improves the actuation response time [12]. On its own, bulk NiTi has good damping properties, but they can be enhanced by the geometrical contribution of a porous structure [7]. Finally, open porosity allows for bone cell ingrowth and reduced stiffness, making porous NiTi ideal for the fabrication of bone implants with improved osseointegration [12,13]. For these reasons, the fabrication of not only porous NiTi structures, but periodic cellular NiTi structures with uniform and predictable properties are highly desirable. Various processing methods have been developed to create such structures with varying degrees of control of pore size, shape, distribution and volume fraction [11,12,14,15]. One as yet unexplored approach for NiTi periodic structures is to weave wires into 3-

dimensional structures as recently demonstrated for Cu and Ni-20Cr wires via a non-crimp 3-D orthogonal weaving technique [16].

While NiTi wires, commercially available with diameters above $\sim 100 \mu\text{m}$, can be woven, the fabrication of NiTi microwires (particularly $< 100 \mu\text{m}$) is difficult [17], and the subsequent weaving of these wires poses a challenge. The low stiffness, high yield stress and/or superelastic behavior of NiTi allows it to sustain the high radii of curvature required for weaving and bending without deforming plastically and, hence, result in weaves that unravel when handled or machined if they are not secured. An alternative approach is to decouple the weaving and alloying steps by depositing a Ti coating of appropriate thickness on a pure Ni wire woven structure via pack cementation (i.e. titanization), and then homogenizing the wires via interdiffusion to obtain near equiatomic NiTi shape memory or superelastic compositions. Therefore, to assess the feasibility of this approach, the present study investigates the homogenization of individual Ti-coated nickel wires and characterizes their microstructure and composition. Furthermore, if proven viable, this titanization/homogenization method could be used on a variety of pure Ni substrates with small characteristic length scales (wires, ribbons, foils, additively manufactured lattices) to fabricate other NiTi geometries,

[☆] Research conducted at Northwestern University, author currently at University of Cincinnati.

* Corresponding author.

E-mail address: Ashley.PazyPuente@uc.edu (A.E. Paz y Puente).

from simple 2D flat springs to complex 3D scaffolds and honeycombs with shape memory and/or superelastic behavior.

Pack cementation is a simple chemical vapor deposition (CVD) process that has been used for over a century to deposit metallic coatings with thicknesses spanning a few to a few hundred micrometers, often with the goal of creating a protective coating with or without interdiffusion with the substrate [18,19]. While pack cementation has been used to deposit mostly Al [20–27], a variety of other elements have been deposited using this method, including Cr [28,29], Mo [30–32], and in a few cases Ti [32–36]. Recently, pack cementation was used to gas-phase alloy Ni-20Cr wire weaves with tailored amounts of Al and Ti such that, upon homogenization, γ' -strengthened Ni-based superalloy woven structures were obtained [36]. Additionally, using a technique similar to pack cementation called powder-immersion-reaction-assisted coating, Mashal et al. titanized and subsequently nitrided a nickel substrate to create a TiN coating for wear and corrosion resistance [37]. In that study, 5 mm thick Ni plates were titanized at temperatures between 750 and 900 °C, which produced a three-layer coating structure composed of Ti₂Ni at the surface, NiTi as an intermediate layer, and Ni₃Ti nearest the Ni substrate. These results suggest that these phases may also be present in the Ti-coated wires investigated in the current study. However, based on previous studies, it can be challenging to eliminate some of these intermediate, brittle intermetallics by subsequent annealing when trying to obtain near equiatomic NiTi [38–40].

Because conventional processing methods require high temperatures (> 1300 °C) and extensive post-processing to achieve sufficient strengthening of the final product [41], several studies have investigated other methods to obtain near equiatomic NiTi, e.g., mechanical alloying of pure Ni and Ti powders or reacting of electrodeposited Ni and Ti layers, which allow more economical fabrication processes compared to traditional fabrication methods such as vacuum induction melting or vacuum arc re-melting [38–40]. For this reason, diffusion in the Ni-Ti binary system has been widely studied. Investigation of the interdiffusion behavior has been conducted with multilayer thin films [42–44], powder compacts [45–48], and electrodeposited structures [38,39,49], all with the aim of achieving near equiatomic NiTi. The results of these studies suggest that the homogenization time and temperature must be chosen carefully to eliminate non-equilibrium intermetallic phases in the final alloy. As early as 1974, Bastin and Rieck [50,51] published a comprehensive study on the formation and growth of various intermetallic phases in Ni-Ti diffusion couples and reported the presence of the Ni(Ti), Ni₃Ti, NiTi, NiTi₂, and Ti(Ni) phases, which are all present in the equilibrium phase diagram [52]. They also calculated diffusion coefficients in various phases and concluded that Ni has a higher intrinsic diffusivity than Ti in Ti(Ni), NiTi₂, and NiTi [51]. A later study reported that Ti diffuses one to two orders of magnitude slower than Ni in NiTi over the temperature range of 675–1000 °C [53]. This imbalance in diffusion coefficients implies that Kirkendall porosity may be observed in this system. In fact, Hassannaemi et al. attributed porosity observed after homogenization of a sample created via the co-electrodeposition of Ni and Ti to the Kirkendall effect [39].

The Kirkendall effect [54] causes the formation of pores near the interface of dissimilar materials during interdiffusion of different atomic species showing an imbalance of diffusivities; the resulting net flux of vacancies can lead to, upon supersaturation, the formation and coalescence of pores [55–59]. Although these Kirkendall pores are usually considered to be detrimental to material properties, they recently were harnessed to form hollow nanoparticles where a single cavity was formed by interdiffusion of Co and O, S, or Se [60]. Several recent studies have investigated this mechanism, though there are only rare examples of metal-metal reactions forming these structures [56,61,62], and none on the Ni-Ti system. While several studies [56,63–70] involving nano-scaled hollow structures exist, few have been performed at the micro-scale: these include the formation of

microshells (hollow spheres) and microcages (hollow cubes or polyhedra) with typical dimensions of 1–30 μm [71–74]. We recently demonstrated that central cavities form via the Kirkendall effect upon homogenization of pack-aluminized Ni-Cr wires with a core/shell structure [75]. Unlike the large number of pores created in diffusion couples with larger volumes, in this case where the wires have diameters of $\sim 75 \mu\text{m}$, the pores coalesce into a single Kirkendall channel due to radial symmetry and spatial confinement. For a dense core-shell structure in which the shell components diffuse slower than the core components, resulting in an inward flux of vacancies toward the center of the structure, similar central Kirkendall porosity could be observed [56,64,67]. Therefore, such internal cavities may be expected to form during homogenization of Ni wires coated with the appropriate amount of Ti to create near equiatomic NiTi, as Ni is known to diffuse faster than Ti [51,53]. The resulting hollow NiTi microtubes would offer additional benefits as compared to NiTi wires, because the surface area to volume ratio would increase and the open porosity could allow for active heating/cooling, making the actuation response faster as the shape memory effect is thermally activated. In the following, the formation and evolution of Kirkendall porosity within Ni wires coated with Ti via pack cementation is discussed together with other microstructural and compositional.

2. Experimental methods

2.1. Processing

2.1.1. Pack titanization

Ni wires (99.99% purity, from Alfa Aesar) with 50 μm initial diameter were titanized via the pack cementation technique. A powder mixture (pack) consisting of 67 wt% inert TiC filler powders (< 44 μm), 30 wt% Ti (< 44 μm , 99.5% purity) source powders, and 3 wt% NH₄Cl activator powders, all procured from Alfa Aesar, was mechanically mixed for ~ 30 min. Twelve 4 cm long wires were embedded in ~ 25 g of pack in an alumina crucible. The filled crucible was then closed with an alumina lid and mounted on a stage at the end of a preheated tube furnace, which was water-chilled to prevent premature activation of the pack. After sealing the tube furnace and flushing with Ar for ~ 15 min, the crucible was inserted into the hot zone for the desired coating time. Based on the Ni-Ti phase diagram [52] and preliminary experimental results for the particular pack composition used in this study, the titanization was conducted at 925 °C, under the lowest eutectic temperature of 942 °C (between Ti and Ti₂Ni), for 2 h to deposit the appropriate amount of Ti. Thereafter, the crucible was retracted back into the water-chilled zone and allowed to cool to near room temperature under continuous Ar flow. Once removed from the tube furnace, the crucible was opened in a glove bag under Ar atmosphere (to prevent the fine redeposited Ti powder from igniting upon exposure to air) and the wires retrieved. The as-coated wires were ultrasonically cleaned in acetone for ~ 5 min to remove pack powders from the surface, and prepared for further heat-treatments and characterization.

2.1.2. Homogenization and aging

Following the pack titanization process, the samples were homogenized so as to obtain single-phase, near-equiatomic NiTi with shape memory or superelastic properties. The same pack titanization conditions (2 h at 925 °C) were used for producing the coating on all of the samples homogenized and presented here. The samples were homogenized at the same temperature as the coating condition (925 °C) for times ranging between 2 and 16 h. To prevent oxidation during homogenization, the wires were vacuum encapsulated in quartz capillaries (0.6 mm ID x 0.8 mm OD) with slivers of Mg ribbon to provide a protective Mg atmosphere upon heating [76]. To investigate the as-coated and homogenized microstructures of the wires, the samples were examined via both traditional metallography techniques and *ex situ* X-ray tomographic microscopy as described in the following section.

2.2. Characterization

2.2.1. Metallography

To observe detailed features of the microstructures and identify and determine compositions of the phase constituents in both the as-coated and homogenized titanized Ni wires, several (3–5) segments from each of a few different wires were mounted in epoxy such that the radial cross-sections were exposed. The samples were metallographically prepared and polished down to 0.05 μm using an alumina suspension. A combination of optical microscopy (OM) and scanning electron microscopy (SEM, Hitachi S-3400N) with energy dispersive X-ray spectroscopy (EDS) were used to characterize the samples.

2.2.2. Ex situ X-ray tomographic microscopy

A series of *ex situ* X-ray tomographic microscopy experiments was conducted to non-destructively evaluate the microstructure of a larger segment of the wires. X-ray tomography scans were collected at the 2-BM beamline of the Advanced Photon Source at Argonne National Laboratory. Each wire was homogenized using the same method described in Section 2.1.2 prior to conducting a room-temperature tomography scan. For the scan, the quartz capillary containing the homogenized Ni-Ti wire was inserted into an alumina sleeve attached to a magnetic base, and mounted on a rotation stage. A schematic of the most relevant components of the experimental setup is shown and described in more detail in Ref. [75]. Tomographic scans were collected using pink beam X-rays with a nominal peak energy of 27 keV and a pco.EDGE camera mounted to a standard microscope with 10 \times magnification (0.65 $\mu\text{m}/\text{px}$) [77]. A series of 750 projections over 180 $^\circ$ of rotation were collected in ~ 30 s (10 ms exposure time). All data were reconstructed using TomoPy as discussed in more details in Ref. [78] from which 2D slices of the ~ 1400 μm longitudinal section of wire within the field-of-view were created. Additionally, a MATLAB script was used to visualize in 3-D the surface of the Kirkendall pores. The pore volume fraction was also calculated in MATLAB by segmenting the pore and wire regions separately and calculating the total number of pixels in each region over the wire length.

3. Results and discussion

3.1. Alloying

3.1.1. Pack titanization

To fully understand the microstructural evolution of the titanized Ni wires, it is critical to characterize the as-coated condition. Because the pack titanization partially consumes the Ni wire (with original diameter of 50 μm) as Ti is deposited from the gas phase and reacts with Ni to form a diffusion coating, the resultant wires had a core/shell structure with an outside diameter of approximately 80 μm depending upon the exact amount of Ti deposited. A low magnification backscattered electron micrograph of a representative, as-coated radial cross-section from a titanized Ni wire is presented in Fig. 1(a) showing two distinct shells around a core. The black spots within the inner shell are TiC particles from the pack that were engulfed during the coating process. A high magnification image of the cross-section is shown in Fig. 1(b) with an overlay of an EDS radial line-scan reporting the corresponding compositions of the shells present. With the combination of the higher magnification and compositional data, it is clear that three intermetallic shells exhibit NiTi₂, NiTi, and Ni₃Ti compositions, in order from surface to inner Ni core. Therefore, each of the three intermetallic phases that exist at 925 $^\circ\text{C}$ in the binary Ni-Ti phase diagram are present in the as-coated wires [52]. Additionally, small acicular precipitates can be seen on the inner side of the intermediate NiTi shell. Based on literature [79–81], these precipitates are likely metastable Ni₄Ti₃ precipitates that formed upon cooling in the tube furnace, as they appear on the Ni-rich side of the NiTi shell and are not present on the Ti-rich side. Given that both the NiTi and Ti-rich Ti₂Ni outermost shells are relatively thick,

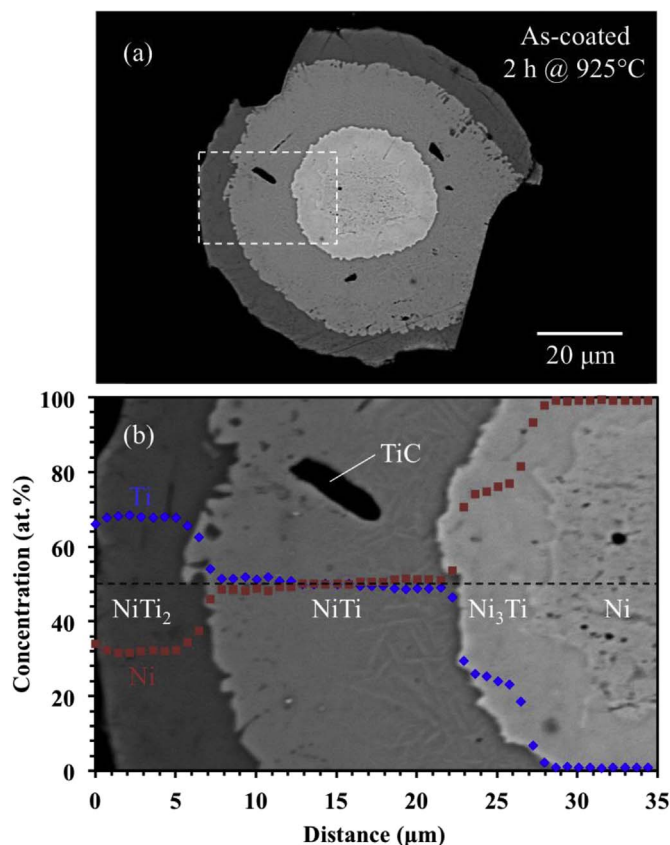


Fig. 1. Backscattered electron micrographs of a radial cross-section from a Ni wire titanized for 2 h at 925 $^\circ\text{C}$ at (a) low magnification where surface damage (missing material at upper left and lower right) is due to metallographic preparation and (b) high magnification with an EDS line scan overlay to show the composition of the core/shell structure.

approximately 15 and 7 μm respectively, it was anticipated that, upon full homogenization the desired near equiatomic NiTi composition would be achieved. In fact, based on area fractions and densities of the phases present, the overall composition was estimated to be 51 at.% Ni and 49 at.% Ti. However, it has been well documented [38–40] that it is difficult to eliminate undesired non-equiatomous intermetallics during solid-state alloying of pure Ni and Ti to obtain single-phase NiTi with shape memory or superelastic properties. Therefore, even if an adequate amount of Ti is deposited on the wires such that the desired average composition is reached, some NiTi₂ and Ni₃Ti may remain and thus prevent full homogenization to near-equiatomous NiTi. The results of the homogenization experiments conducted on the wires in this study are presented in the following section.

3.1.2. Homogenization

With the as-coated microstructure established, several pack-titanized wires were annealed at 925 $^\circ\text{C}$ for various times ranging from 2 to 16 h to assess the microstructural evolution during homogenization. No significant difference in the microstructure, both in terms of phase constituents and pores, was observed between 2 and 16 h. The structure appears to be fully homogenized by 4 h, but pores have typically developed by 2 h and remain stable up to 16 h. A representative radial cross-section of a wire homogenized for 4 h is illustrated in Fig. 2. In the optical micrograph shown in Fig. 2(a), the cross-section appears to be single phase with a large (~ 25 μm diameter) pore with near-circular cross-section close to the center. Kirkendall porosity is expected as Ni has a higher intrinsic diffusivity than Ti in the NiTi phase [51,53]; the coalescence of the pores into a single cavity is due to radial symmetry and spatial confinement of the wire. Therefore, because of the concentration gradient present in the as-coated core/shell structure, Ni

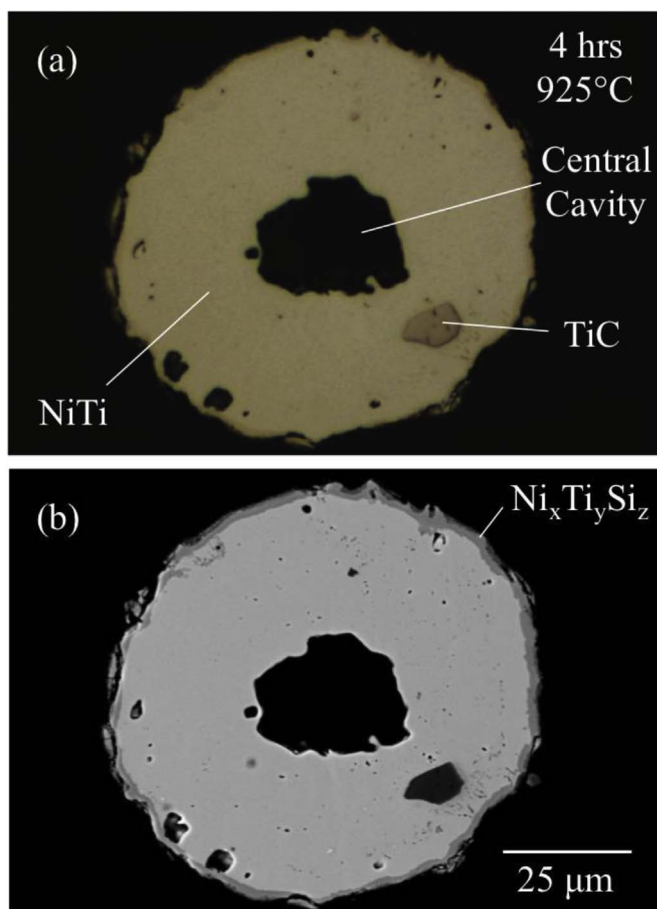


Fig. 2. Low magnification (a) optical and (b) backscattered electron micrographs of a radial cross section of a titanized Ni wire following homogenization for 4 h at 925 °C.

diffuses radially out from the core faster than Ti replaces it during homogenization, leading to accumulation and eventual supersaturation of vacancies followed by formation of the central Kirkendall pore. As previously mentioned, during the titanization process some TiC particles were engulfed by the growing diffusion coating and remain embedded in the wires after homogenization as labeled in Fig. 2(a). The smaller pores near the surface are likely from pull-out of engulfed TiC particles upon metallographic preparation of the cross-section and are not expected to originate from the Kirkendall effect.

To confirm the composition and uniformity of the homogenized titanized Ni wires, SEM/EDS was conducted on the same exact cross-section in the optical micrograph in Fig. 2(a), as shown in Fig. 2(b) in a backscattered electron micrograph. A thin outer shell is visible, that is not apparent in the optical image of Fig. 2(a) and is determined by EDS analysis to be a ternary silicide containing approximately 48 at.% Ti, 33 at.% Ni and 19 at.% Si, and is thus likely $\text{Ni}_3\text{Ti}_2\text{Si}$ according to the phase diagram [82] and labeled $\text{Ni}_x\text{Ti}_y\text{Si}_z$ in Fig. 2(b). The average composition of the predominant phase present in the cross-section in Fig. 2(b) was measured to be 51.6 at.% Ni and 48.4 at.% Ti. The composition was nearly constant (± 0.5 at. %) throughout the NiTi portion of the same cross-section as observed from the EDS line scan conducted at a higher magnification, as presented in Fig. 3(a). Two other cross-sections from the same wire were also analyzed and had similar microstructures to the one shown in Fig. 2 including the large central Kirkendall pore; however, the compositions were slightly different with average Ti contents of 49.4 and 50.1 at.%, respectively. Therefore, the majority phase constituent of these three cross-sections annealed at 925 °C is indeed near equiatomic NiTi, as indicated by the red oval on the binary Ni-Ti phase diagram shown in Fig. 3(b). While

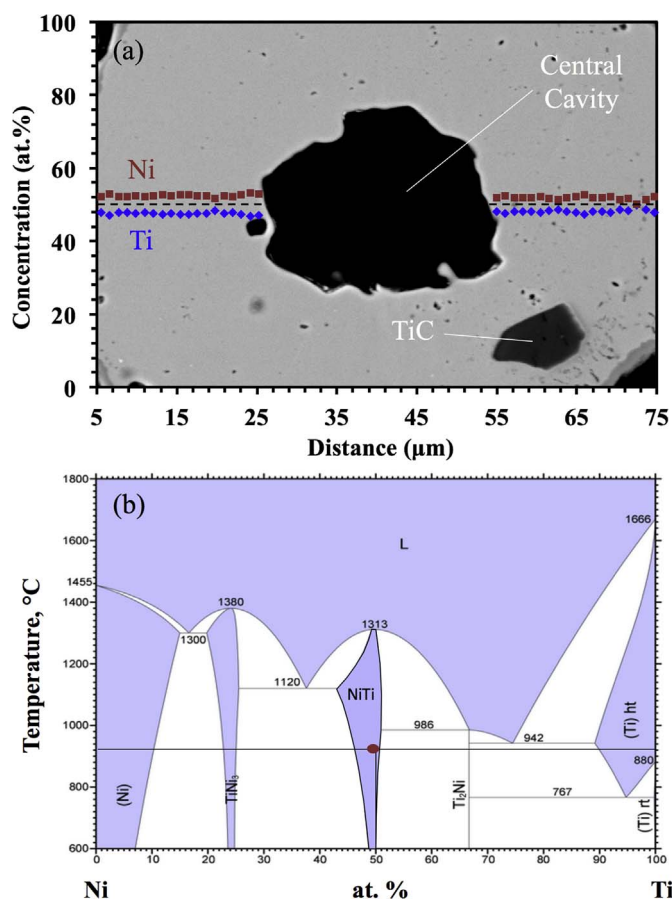


Fig. 3. (a) High magnification backscatter electron micrograph of the cross-section shown in Fig. 2 with an EDS line scan showing a uniform composition and (b) a binary Ni-Ti phase diagram [52] with a horizontal black line indicating the homogenization temperature, a vertical black line indicating the equiatomic NiTi composition, and the red oval representing the range of compositions measured for three different cross-sections from the same titanized Ni wire. (For interpretation of the references to colour in this figure legend, the reader is referred to the web version of this article.)

the NiTi compositions were determined to be relatively uniform throughout a particular cross-section, the compositional variation among different regions of the wire, likely due to slight variations in coating thickness during deposition, is significant considering the steep change in martensite start transformation temperatures as a function of composition [46]. At room temperature, Ni-rich compositions are superelastic while Ti-rich compositions are shape memory. Therefore, while thermal-mechanical testing is not presented here, given the variations in composition (49–53 at.% Ni) for the cross-sections measured, mixed superelastic and shape-memory behavior can be expected within a particular wire. The cross-section shown in Figs. 2 and 3 was representative of many of the cross-sections observed in other wires as well. However, some showed a small region of Ni_3Ti remaining near the central pore of the remainder of the cross-section consisting of slightly more Ni-rich (~ 53 at.% Ni) NiTi with no significant concentration gradient. Given that the NiTi phase present in these Ni_3Ti -containing cross-sections had a constant composition of the tie line value between NiTi and Ni_3Ti [52], it appears that equilibrium has been reached and not quite enough Ti was deposited during titanization to transform these particular cross-sections to single-phase NiTi.

3.1.3. Kirkendall pore evolution

To study the Kirkendall porosity, room temperature tomographic scans were collected of three different wires annealed for 2, 4 and 8 h at 925 °C. A 2D radiograph of a 1400 μm section of each of the three wires is shown in Fig. 4(a–c). Portions of the wires observed were not straight,

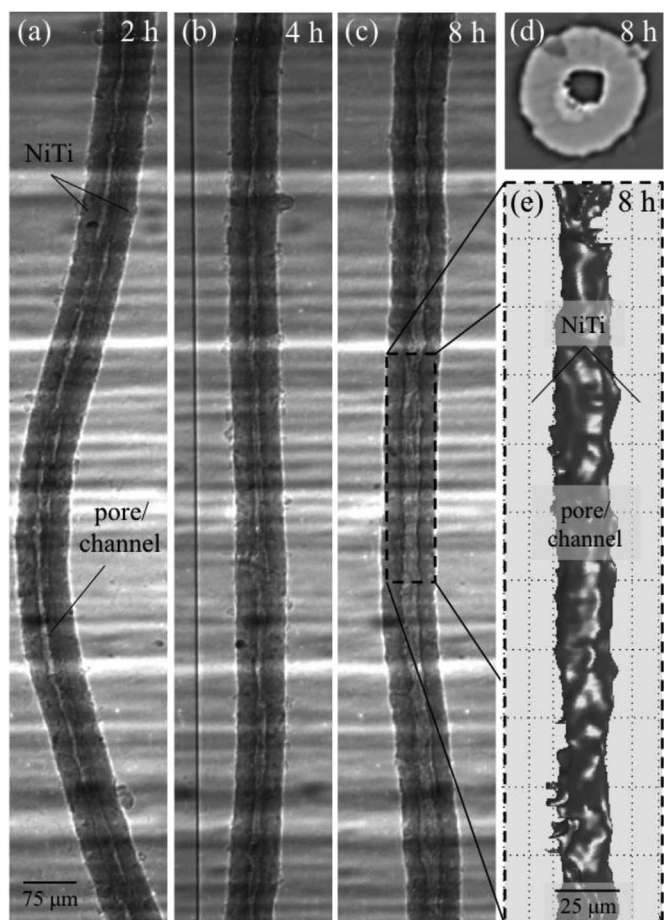


Fig. 4. Radiographs of titanized Ni wires homogenized for (a) 2, (b) 4, and (c) 8 h at 925 °C showing central Kirkendall channels. (d) A representative reconstructed slice and (e) a 3D visualization of a segment of the Kirkendall channel surface from the microtube shown in (c).

as illustrated in Fig. 4(a), as the wires became wavy upon titanization due to plastic relaxation of internal stresses created by the growth of Ni-Ti intermetallic phases. From the radiographs, it is apparent that Kirkendall porosity has developed within all of them along the entire length captured within the field of view and seems to form one continuous cylindrical channel, particularly in the sample annealed for 8 h as shown in Fig. 4(c). A reconstructed slice from the wire in Fig. 4(c) is presented in Fig. 4(d) showing a representative radial cross-section. The dark region in the center represents the Kirkendall porosity present within this cross-section. The brighter region near the pore is Ni₃Ti and the darker spots on the surface are embedded TiC particles, with these features identified based on observation of metallographically prepared cross-sections. From the series of reconstructed radial cross-sections, a segment of the surface of the Kirkendall channel was visualized in 3-D as shown in Fig. 4(e). It is apparent that the surface of the long cylindrical channel is rougher than the tomographic resolution, and is indeed continuous through this portion of the wire. The measured pore volume fraction based on the 3D visualization is approximately 7.5%. Given that the channel is continuous over the length of the field of view (1400 μm) and the diameter of this wire is approximately 78 μm, the aspect ratio of the tube as a whole in this case is almost 18. If just the Kirkendall channel is considered, with a diameter of approximately 22 μm, the aspect ratio is about 64. In fact, while a maximum tube length was not determined, it appears from the radiographs of these samples that the channel remains continuous well past the edge of the field of view on either side making these true microtubes.

To further investigate the early development of the Kirkendall

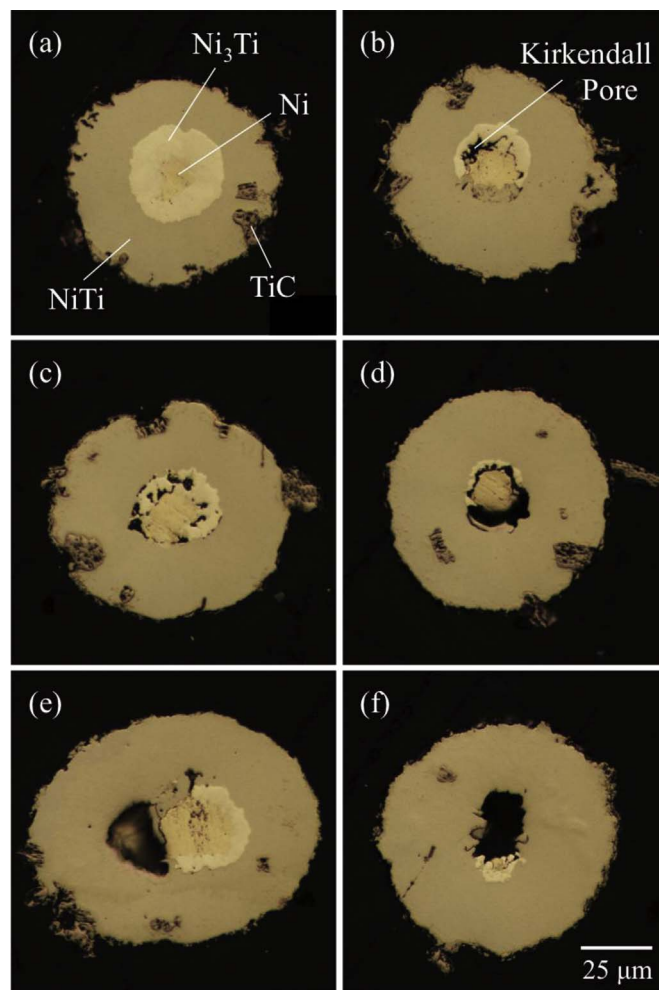


Fig. 5. Optical micrographs of six different cross-sections (a)–(f) from two different titanized Ni wires that were homogenized for 2 h at 925 °C showing the variation in Kirkendall porosity location and area fraction.

porosity, two wires homogenized for 2 h at 925 °C, including the one shown in Fig. 4(a), were cross-sectioned and metallographically prepared. Fig. 5(a)–(f) are optical micrographs of six different cross-sections obtained from these two wires. In all six images, some of the original Ni core and the Ni₃Ti reaction layer formed in the diffusion coating still remain. It appears that numerous Kirkendall pores actually formed at both the NiTi/Ni₃Ti and Ni₃Ti/Ni interfaces as illustrated most clearly in Fig. 5(c) suggesting there is an imbalance in the intrinsic diffusivities of Ni and Ti in both NiTi/Ni₃Ti and Ni₃Ti/Ni couples. Additionally, this cross-section indicates that the pores start forming somewhat symmetrically about the Ni-core, and then likely merge into a few, or a single, large centrally located pore as homogenization progresses. As discussed for the case of aluminized Ni-Cr wires subjected to homogenization in Ref. [75], there is a tendency for the Kirkendall pores to develop a crescent-shaped cross-section as one large pore forms at the core/shell interface and grows at the expense of smaller pores as it acts as a vacancy sink. Once a large pore forms around the interface it also acts as a diffusion barrier as it interrupts the direct diffusion between the Ni-core and the shell and lengthens the diffusion path for homogenization to proceed. In the ternary Ni-Cr-Al case, Ni₃Al did not form, at least at an observable thickness, due to the low solubility of Cr within this phase. However, the Kirkendall porosity also formed near the interface between the near equiatomic NiAl phase and the remaining Ni-Cr core similar to what is observed here for the Ni-Ti wires. Also, in the Ni-Cr-Al system, chromium aluminide precipitates formed near the center of the wires which prevented the Kirkendall pores from

smoothing via surface diffusion; by contrast, in the present binary Ni-Ti system no insoluble phase is present to inhibit the full cylindrical shape of the pore at long annealing times.

4. Conclusions

Through the pack titanization of pure Ni wires with an initial diameter of 50 μm and the subsequent homogenization of the resulting ~ 80 μm diameter Ni-Ti wires, near equiatomic NiTi microtubes were fabricated. The following conclusions are reached:

1. Pack titanization of Ni wires for 2 h at 925 $^{\circ}\text{C}$ produces a Ni/Ni₃Ti/NiTi/NiTi₂ core/tri-shell structure.
2. During early stages of homogenization, Kirkendall pores form somewhat symmetrically at both the NiTi/Ni₃Ti and Ni₃Ti/Ni interfaces. After full homogenization, these pores coalesce into a single continuous channel, thus creating microtubes.
3. While the composition is essentially constant single-phase near-equiatomic NiTi across a particular cross-section, significant compositional fluctuations (49–53 at.% Ni) exist within an individual NiTi microtube, most probably due to small variations in initial coating thickness.

Overall, pack titanization of 50 μm Ni wires can be used to produce single-phase, near-equiatomic NiTi microtubes where, because the diffusion distances are small, other intermetallics can be eliminated given a sufficient Ti deposition and anneal time. However, due to a not perfectly uniform coating thickness, compositional fluctuations are present, which would lead to a range of shape memory and superelastic behavior.

Acknowledgements

AEPyP acknowledges the National Science Foundation Graduate Research Fellowship Program for funding support. The authors acknowledge the financial support from the Defense Advanced Research Projects Agency under award number W91CRB1010004 (Dr. Judah Goldwasser, program manager). They also thank Profs. Peter Voorhees and David Seidman (Northwestern University) for their helpful discussions, Dr. Dinc Erdeniz, and Ms. Shannon Taylor, Victoria Vaccarrea, and Sarah Plain (Northwestern University) for experimental assistance at APS, and Dr. Ashwin Shahani (Northwestern University) for assistance with the MATLAB script for 3-D visualization and measuring pore volume fraction. This work made use of the EPIC, Keck-II, and/or SPID facility(ies) of Northwestern University's NUANCE Center, which has received support from the Soft and Hybrid Nanotechnology Experimental (SHyNE) Resource (NSF ECCS-1542205); the MRSEC program (NSF DMR-1121262) at the Materials Research Center; the International Institute for Nanotechnology (IIN); the Keck Foundation; and the State of Illinois, through the IIN. This work also made use of the OMM facility which receives support from the MRSEC Program (NSF DMR-1121262) of the Materials Research Center at Northwestern University.

References

- [1] W.J. Buehler, J.V. Gilfrich, R.C. Wiley, Effect of low-temperature phase changes on the mechanical properties of alloys near composition TiNi, *J. Appl. Phys.* 34 (1963) 1475–1477, <http://dx.doi.org/10.1063/1.1729603>.
- [2] G.L. Hofman, L.C. Walters, T.H. Bauer, Metallic fast reactor fuels, *Prog. Nucl. Energy* 31 (1997) 83–110, [http://dx.doi.org/10.1016/0149-1970\(96\)00005-4](http://dx.doi.org/10.1016/0149-1970(96)00005-4).
- [3] C.D.J. Barras, K.A. Myers, Nitinol - Its use in vascular surgery and other applications, *EJVES Extra* 19 (2010) 564–569, <http://dx.doi.org/10.1053/ejvs.2000.1111>.
- [4] J. Van Humbeeck, Non-medical applications of shape memory alloys, *Mater. Sci. Eng. A* 273–275 (1999) 134–148, [http://dx.doi.org/10.1016/S0921-5093\(99\)00293-2](http://dx.doi.org/10.1016/S0921-5093(99)00293-2).
- [5] T. Duerig, A. Pelton, D. Stöckel, An overview of nitinol medical applications, *Mater. Sci. Eng. A* 273–275 (1999) 149–160, [http://dx.doi.org/10.1016/S0921-5093\(99\)00294-4](http://dx.doi.org/10.1016/S0921-5093(99)00294-4).
- [6] J. Mohd Jani, M. Leary, A. Subic, M.A. Gibson, A review of shape memory alloy research, applications and opportunities, *Mater. Des.* 56 (2014) 1078–1113, <http://dx.doi.org/10.1016/j.matdes.2013.11.084>.
- [7] M.A. Qidwai, P.B. Entchev, D.C. Lagoudas, V.G. DeGiorgi, Modeling of the thermomechanical behavior of porous shape memory alloys, *Int. J. Solids Struct.* 38 (2001) 8653–8671, [http://dx.doi.org/10.1016/S0020-7683\(01\)00118-4](http://dx.doi.org/10.1016/S0020-7683(01)00118-4).
- [8] Y. Zhao, M. Taya, H. Izui, Study on energy absorbing composite structure made of concentric NiTi spring and porous NiTi, *Int. J. Solids Struct.* 43 (2006) 2497–2512, <http://dx.doi.org/10.1016/j.ijsolstr.2005.06.043>.
- [9] S.A. Shabalovskaya, Surface, corrosion and biocompatibility aspects of Nitinol as an implant material, *Biomed. Mater. Eng.* 12 (2002) 69–109.
- [10] D.J. Blackwood, Biomaterials: past successes and future problems, *Corros. Rev.* 21 (2003) 97–124, <http://dx.doi.org/10.1515/CORRREV.2003.21.2-3.97>.
- [11] A. Bansiddhi, T.D. Sargeant, S.I. Stupp, D.C. Dunand, Porous NiTi for bone implants: a review, *Acta Biomater.* 4 (2008) 773–782, <http://dx.doi.org/10.1016/j.actbio.2008.02.009>.
- [12] C. Bewerse, L.C. Brinson, D.C. Dunand, NiTi with 3D-interconnected microchannels produced by liquid phase sintering and electrochemical dissolution of steel tubes, *J. Mater. Process. Technol.* 214 (2014) 1895–1899, <http://dx.doi.org/10.1016/j.jmatprotec.2014.04.006>.
- [13] V. Karageorgiou, D. Kaplan, Porosity of 3D biomaterial scaffolds and osteogenesis, *Biomaterials* 26 (2005) 5474–5491, <http://dx.doi.org/10.1016/j.biomaterials.2005.02.002>.
- [14] G. Ryan, A. Pandit, D.P. Apatsidis, Fabrication methods of porous metals for use in orthopaedic applications, *Biomaterials* 27 (2006) 2651–2670, <http://dx.doi.org/10.1016/j.biomaterials.2005.12.002>.
- [15] M.B. Nasab, M.R. Hassan, B.B. Sahari, Metallic biomaterials of knee and hip - A review, *Trends Biomater. Artif. Organs* 24 (2010) 69–82.
- [16] L. Zhao, S. Ha, K.W. Sharp, A.B. Geltmacher, R.W. Fonda, A.H. Kinsey, et al., Permeability measurements and modeling of topology-optimized metallic 3-D woven lattices, *Acta Mater.* 81 (2014) 326–336, <http://dx.doi.org/10.1016/j.actamat.2014.08.037>.
- [17] D.A. Miller, D.C. Lagoudas, Influence of cold work and heat treatment on the shape memory effect and plastic strain development of NiTi, *Mater. Sci. Eng. A* 308 (2001) 161–175, [http://dx.doi.org/10.1016/S0921-5093\(00\)01982-1](http://dx.doi.org/10.1016/S0921-5093(00)01982-1).
- [18] T. Van Aller, No. US 1,155,974, 1911.
- [19] E.G. Gilson, No. US 1,091,057, 1913.
- [20] D. Erdeniz, D.C. Dunand, Microstructure development during pack aluminization of nickel and nickel-chromium wires, *Intermetallics* 50 (2014) 43–53, <http://dx.doi.org/10.1016/j.intermet.2014.02.009>.
- [21] G.W. Goward, L.W. Cannon, Pack cementation coatings for superalloys: a review of history, theory, and practice, *J. Eng. Gas Turbines Power* 110 (1988) 150, <http://dx.doi.org/10.1115/1.3240078>.
- [22] G.W. Goward, D.H. Boone, Mechanisms of formation of diffusion aluminide coatings on nickel-base superalloys, *Oxid. Met.* 3 (1971) 475–495, <http://dx.doi.org/10.1007/BF00604047>.
- [23] R. Pichoir, Influence of the mode of formation on the oxidation and corrosion behavior of NiAl-type protective coatings, *Mater. Coatings to Resist High Temp. Corros. Applied Science Publisher, London*, 1978, pp. 271–292.
- [24] A.J. Hickl, R.W. Heckel, Kinetics of phase layer growth during aluminide coating of nickel, *Metall. Trans. A* 6 (1975) 431–440, <http://dx.doi.org/10.1007/BF02658400>.
- [25] D.K. Das, V. Singh, S.V. Joshi, Evolution of aluminide coating microstructure on nickel-base cast superalloy CM-247 in a single-step high-activity aluminizing process, *Metall. Mater. Trans. A* 29A (1998) 2173–2188.
- [26] D.C. Tu, L.L. Seigle, Kinetics of formation and microstructure of aluminide coatings on Ni-Cr alloys, *Thin Solid Films* 95 (1982) 47–56.
- [27] R. Sakidja, F. Rioult, J. Werner, J.H. Perepezko, Aluminum pack cementation of Mo-Si-B alloys, *Scr. Mater.* 55 (2006) 903–906, <http://dx.doi.org/10.1016/j.scriptamat.2006.07.044>.
- [28] R. Mévrel, C. Duret, R. Pichoir, Pack cementation processes, *Mater. Sci. Technol.* 2 (1986) 201–206, <http://dx.doi.org/10.1179/026708386790123297>.
- [29] H. Choe, D.C. Dunand, Synthesis, structure, and mechanical properties of Ni-Al and Ni-Cr-Al superalloy foams, *Acta Mater.* 52 (2004) 1283–1295, <http://dx.doi.org/10.1016/j.actamat.2003.11.012>.
- [30] J. Li, C. Xia, Y. Gu, Effect of temperature on microstructure of molybdenum diffusion coating on titanium substrate, *J. Cent. South Univ. Technol.* 11 (2004) 15–18, <http://dx.doi.org/10.1007/s11771-004-0003-8>.
- [31] C. Wang, D.C. Dunand, Concurrent growth of Kirkendall pores and vapor-solid-solid protuberances on Ni wires during Mo vapor-phase deposition, *Metall. Mater. Trans. A* 45 (2014) 6252–6259, <http://dx.doi.org/10.1007/s11661-014-2587-4>.
- [32] C. Wang, D.C. Dunand, Microstructure evolution during Al, Ti, and Mo surface deposition and volume diffusion in Ni-20Cr wires and woven structures, *Metall. Mater. Trans. A* 46 (2015) 2249–2254, <http://dx.doi.org/10.1007/s11661-015-2794-7>.
- [33] M.R. Bateni, S. Mirdamadi, F. Ashrafzadeh, J.A. Szpunar, R.A.L. Drew, Oxidation behaviour of titanium coated copper substrate, *Surf. Coat. Technol.* 139 (2001) 192–199, [http://dx.doi.org/10.1016/S0257-8972\(01\)00990-2](http://dx.doi.org/10.1016/S0257-8972(01)00990-2).
- [34] M. Britchi, N. Ene, M. Olteanu, C. Radovici, Titanium diffusion coatings on austenitic steel obtained by the pack cementation method, *J. Serbian Chem. Soc.* 74 (2009) 203–212, <http://dx.doi.org/10.2298/JSC0902203B>.
- [35] F.S. Nogorani, F. Ashrafzadeh, A. Saatchi, Microstructural analysis and growth mechanism of single-step aluminum-titanium diffusion coatings on a nickel-based substrate, *Surf. Coat. Technol.* 210 (2012) 97–102, <http://dx.doi.org/10.1016/j.surfcoat.2012.08.071>.

- [36] D. Erdeniz, K.W. Sharp, D.C. Dunand, Transient liquid-phase bonded 3D woven Ni-based superalloys, *Scr. Mater.* 108 (2015) 60–63, <http://dx.doi.org/10.1016/j.scriptamat.2015.06.016>.
- [37] I. Mashal, L. Klinger, I. Gotman, E.Y. Gutmanas, Titanium nitride coating on nickel produced by a powder immersion reaction-assisted coating method, *Surf. Coat. Technol.* 200 (2006) 3561–3566, <http://dx.doi.org/10.1016/j.surfcoat.2004.10.123>.
- [38] S. Srikomol, Y. Boonyongmaneerat, R. Techapiesancharoenkij, Electrochemical codeposition and heat treatment of nickel-titanium alloy layers, *Metall. Mater. Trans. B* 44 (2013) 53–62, <http://dx.doi.org/10.1007/s11663-012-9747-y>.
- [39] V. Hasannaemi, T. Shahrabi, S. Sanjabi, Fabrication of NiTi layer via co-electrodeposition of nickel and titanium, *Surf. Coat. Technol.* 210 (2012) 10–14, <http://dx.doi.org/10.1016/j.surfcoat.2012.07.054>.
- [40] Y.W. Gu, C.W. Goh, L.S. Goi, C.S. Lim, A.E.W. Jarfors, B.Y. Tay, et al., Solid state synthesis of nanocrystalline and/or amorphous 50Ni–50Ti alloy, *Mater. Sci. Eng. A* 392 (2005) 222–228, <http://dx.doi.org/10.1016/j.msea.2004.09.025>.
- [41] M.H. Wu, Fabrication of nitinol materials and components, *Proc. Int. Conf. Shape Mem. Superelastic Technol.* (2001) 285–292.
- [42] T. Lehnert, H. Grimmer, P. Böni, M. Horisberger, R. Gotthardt, T. Lehnert, et al., Characterization of shape-memory alloy thin films made up from sputter-deposited Ni/Ti multilayers, *Acta Mater.* 48 (2000) 4065–4071, [http://dx.doi.org/10.1016/S1359-6454\(00\)00189-0](http://dx.doi.org/10.1016/S1359-6454(00)00189-0).
- [43] S. Singh, S. Basu, P. Bhatt, A.K. Poswal, Kinetics of alloy formation at the interfaces in a Ni-Ti multilayer: X-ray and neutron reflectometry study, *Phys. Rev. B* 79 (2009), <http://dx.doi.org/10.1103/PhysRevB.79.195435>.
- [44] X. Shao, X. Guo, Y. Han, Z. Lin, J. Qin, W. Lu, et al., Preparation of TiNi films by diffusion technology and the study of the formation sequence of the intermetallics in Ti-Ni systems, *J. Mater. Res.* 29 (2014) 2707–2716, <http://dx.doi.org/10.1557/jmr.2014.264>.
- [45] J.S. Kim, J.H. Kang, S.B. Kang, K.S. Yoon, Y.S. Kwon, Porous TiNi biomaterial by self-propagating high-temperature synthesis, *Adv. Eng. Mater.* 6 (2004) 403–406, <http://dx.doi.org/10.1002/adem.200405151>.
- [46] J. Mentz, J. Frenzel, M.F.X. Wagner, K. Neuking, G. Eggeler, H.P. Buchkremer, et al., Powder metallurgical processing of NiTi shape memory alloys with elevated transformation temperatures, *Mater. Sci. Eng. A* 491 (2008) 270–278, <http://dx.doi.org/10.1016/j.msea.2008.01.084>.
- [47] D. Cluff, S.F. Corbin, The influence of Ni powder size, compact composition and sintering profile on the shape memory transformation and tensile behaviour of NiTi, *Intermetallics* 18 (2010) 1480–1490, <http://dx.doi.org/10.1016/j.intermet.2010.03.043>.
- [48] M.H. Ismail, R. Goodall, H.A. Davies, I. Todd, Porous NiTi alloy by metal injection moulding/sintering of elemental powders: effect of sintering temperature, *Mater. Lett.* 70 (2012) 142–145, <http://dx.doi.org/10.1016/j.matlet.2011.12.008>.
- [49] A. Robin, Behavior of titanium electrocoatings on nickel in fluoride melts, *Mater. Lett.* 34 (1998) 196–201, [http://dx.doi.org/10.1016/S0167-577x\(97\)00166-3](http://dx.doi.org/10.1016/S0167-577x(97)00166-3).
- [50] G.F. Bastin, G.D. Rieck, Diffusion in titanium-nickel system. 1. Occurrence and growth of various intermetallic compounds, *Metall. Trans.* 5 (1974) 1817–1826, <http://dx.doi.org/10.1007/bf02644146>.
- [51] G.F. Bastin, G.D. Rieck, Diffusion in titanium-nickel system. 2. Calculations of chemical and intrinsic diffusion-coefficients, *Metall. Trans.* 5 (1974) 1827–1831, <http://dx.doi.org/10.1007/bf02644147>.
- [52] P. Bellen, K.C. Hari Kumar, P. Wollants, Thermodynamic assessment of the Ni-Ti phase diagram, *Z. Für Met.* 87 (1996) 972–978.
- [53] S. V Divinski, I. Stloukal, L. Kral, C. Herzig, Diffusion of titanium and nickel in B2 NiTi, *Defect Diffus. Forum.* 289–292 (2009) 377–382 doi:10.4028/www.scientific.net/DDF.289-292.377.
- [54] A.D. Smigelskas, E.O. Kirkendall, Zinc diffusion in alpha brass, *Trans. Am. Inst. Min. Metall. Pet. Eng.* 171 (1947) 130–142.
- [55] F. Seitz, On the porosity observed in the Kirkendall effect, *Acta Metall.* 1 (1953) 355–369, [http://dx.doi.org/10.1016/0001-6160\(53\)90112-6](http://dx.doi.org/10.1016/0001-6160(53)90112-6).
- [56] H.J. Fan, U. Gösele, M. Zacharias, Formation of nanotubes and hollow nanoparticles based on Kirkendall and diffusion processes: a review, *Small* 3 (2007) 1660–1671, <http://dx.doi.org/10.1002/smll.200700382>.
- [57] K.J. Zeng, R. Stierman, T.C.C. Chiu, D. Edwards, K. Ano, K.N.N. Tu, Kirkendall void formation in eutectic SnPb solder joints on bare Cu and its effect on joint reliability, *J. Appl. Phys.* 97 (2005), <http://dx.doi.org/10.1063/1.1839637>.
- [58] H. Schroder, K. Samwer, U. Koster, H. Schröder, K. Samwer, U. Köster, Micromechanism for metallic-glass formation by solid-state reactions, *Phys. Rev. Lett.* 54 (1985) 197–200, <http://dx.doi.org/10.1103/PhysRevLett.54.197>.
- [59] Z. Radi, P.B. Barna, J. Labar, Kirkendall voids and the formation of amorphous phase in the AlPt thin film system prepared by high temperature successive deposition, *J. Appl. Phys.* 79 (1996) 4096–4100, <http://dx.doi.org/10.1063/1.361772>.
- [60] Y.D. Yin, R.M.M. Rioux, C.K.K. Erdonmez, S. Hughes, G.A. Somorjai, A.P.P. Alivisatos, Formation of hollow nanocrystals through the nanoscale Kirkendall effect, *Science* 304 (2004) 711–714, <http://dx.doi.org/10.1126/science.1096566>.
- [61] H.-P. Liang, Y.-G. Guo, H.-M. Zhang, J.-S. Hu, L.-J. Wan, C.-L. Bai, Controllable AuPt bimetallic hollow nanostructures, *Chem. Commun. (Camb)* (13) (2004) 1496–1497, <http://dx.doi.org/10.1039/b402745k>.
- [62] S.H. Zhou, B. Varughese, B. Eichhorn, G. Jackson, K. McIlwrath, Pt-Cu core-shell and alloy nanoparticles for heterogeneous NO_x reduction: anomalous stability and reactivity of a core-shell nanostructure, *Angew. Chem. Int. Ed.* 44 (2005) 4539–4543, <http://dx.doi.org/10.1002/anie.200500919>.
- [63] Q.G. Li, R.M. Penner, Photoconductive cadmium sulfide hemicylindrical shell nanowire ensembles, *Nano Lett.* 5 (2005) 1720–1725, <http://dx.doi.org/10.1021/nl050994x>.
- [64] H.J. Fan, M. Knez, R. Scholz, K. Nielsch, E. Pippel, D. Hesse, et al., Monocrystalline spinel nanotube fabrication based on the Kirkendall effect, *Nat. Mater.* 5 (2006) 627–631, <http://dx.doi.org/10.1038/nmat1673>.
- [65] H. Tan, S. Li, W.Y. Fan, Core-shell and hollow nanocrystal formation via small molecule surface photodissociation; Ag@Ag₂Se as an example, *J. Phys. Chem. B* 110 (2006) 15812–15816, <http://dx.doi.org/10.1021/jp0616011>.
- [66] C. Hwee, B. Ng, H. Tan, W.Y. Fan, Formation of Ag 2 Se nanotubes and dendrite-like structures from UV irradiation of a CSe 2/Ag colloidal solution, *Langmuir* 22 (2006) 9712–9717.
- [67] J. Zhou, J. Liu, X. Wang, J. Song, R. Tummala, N.S. Xu, et al., Vertically aligned Zn₂SiO₄ nanotube/ZnO nanowire heterojunction arrays, *Small* 3 (2007) 622–626, <http://dx.doi.org/10.1002/smll.200600495>.
- [68] X. Chen, Z. Zhang, Z. Qiu, C. Shi, X. Li, Hydrothermal fabrication and characterization of polycrystalline linneite (Co₃S₄) nanotubes based on the Kirkendall effect, *J. Colloid Interface Sci.* 308 (2007) 271–275, <http://dx.doi.org/10.1016/j.jcis.2006.12.054>.
- [69] Y. Chang, M.L. Lye, H.C. Zeng, Large-scale synthesis of high-quality ultralong copper nanowires, *Langmuir* 21 (2005) 3746–3748, <http://dx.doi.org/10.1021/la050220w>.
- [70] Q. Wang, J.-X. Li, G.-D. Li, X.-J. Cao, K.-J. Wang, J.-S. Chen, Formation of CuS nanotube arrays from CuCl Nanorods through a gas-solid reaction route, *J. Cryst. Growth* 299 (2007) 386–392, <http://dx.doi.org/10.1016/j.jcrysgro.2006.11.304>.
- [71] F. Aldinger, Controlled porosity by an extreme Kirkendall effect, *Acta Metall.* 22 (1974) 923–928, [http://dx.doi.org/10.1016/0001-6160\(74\)90059-5](http://dx.doi.org/10.1016/0001-6160(74)90059-5).
- [72] H.J. Fan, R. Scholz, F.M. Kolb, M. Zacharias, U. Gösele, Growth mechanism and characterization of zinc oxide microcages, *Solid State Comm.* 130 (2004) 517–521, <http://dx.doi.org/10.1016/j.ssc.2004.03.014>.
- [73] L. Ye, C. Wu, W. Guo, Y. Xie, MoS₂ hierarchical hollow cubic cages assembled by bilayers: one-step synthesis and their electrochemical hydrogen storage properties, *Chem. Comm. (Camb)* 2 (2006) 4738–4740, <http://dx.doi.org/10.1039/b610601c>.
- [74] C. Guo, G. Zhang, Z. Shen, P. Sun, Z. Yuan, Q. Jin, et al., Hydrothermal synthesis and formation mechanism of micrometer-sized MoO₂ hollow spheres, *Chin. J. Chem. Phys.* 19 (2006) 543–548, [http://dx.doi.org/10.1360/cjcp2006.19\(6\).543.6](http://dx.doi.org/10.1360/cjcp2006.19(6).543.6).
- [75] A.E. Paz y Puente, D. Erdeniz, J.L. Fife, D.C. Dunand, In situ X-ray tomographic microscopy of Kirkendall pore formation and evolution during homogenization of pack-aluminized Ni-Cr wires, *Acta Mater.* 103 (2016) 534–546, <http://dx.doi.org/10.1016/j.actamat.2015.10.013>.
- [76] T. Aydoğmuş, Ş. Bor, Enhanced sintering of TiNi shape memory foams under Mg vapor atmosphere, *Metall. Mater. Trans. A* 43 (2012) 5173–5181, <http://dx.doi.org/10.1007/s11661-012-1350-y>.
- [77] X. Xiao, F. Füsseis, F. De Carlo, X-ray fast tomography and its applications in dynamical phenomena studies in geosciences at Advanced Photon Source, *Proc. Spie.* 8506 (2012), <http://dx.doi.org/10.1117/12.936331> 85060K.
- [78] D. Gürsoy, F. De Carlo, X. Xiao, C. Jacobsen, TomoPy: a framework for the analysis of synchrotron tomographic data, *J. Synchrotron Radiat.* 21 (2014) 1188–1193, <http://dx.doi.org/10.1107/S1600577514013939>.
- [79] H. Zhao, C.Q. Liang, J.T. Liu, Y.X. Tong, F. Chen, B. Tian, et al., Effect of aging treatment on superelasticity of a Ti_{48.8}Ni_{50.8}VO₄ alloy, *J. Mater. Eng. Perform.* 21 (2012) 2566–2571, <http://dx.doi.org/10.1007/s11665-012-0373-2>.
- [80] C.L. Chu, J.C. Chung, P.K. Chu, Effects of heat treatment on characteristics of porous Ni-rich NiTi SMA prepared by SHS technique, *Trans. Nonferrous Met. Soc. China (English Ed.)* 16 (2006) 49–53, [http://dx.doi.org/10.1016/S1003-6326\(06\)60009-5](http://dx.doi.org/10.1016/S1003-6326(06)60009-5).
- [81] G. Eggeler, J. Michutta, C. Somsen, K. Neuking, A. Yawny, Y.I.I. Chumlyakov, Process of 30 mm diameter cylindrical Ni-rich NiTi single crystals with one family of Ni₄Ti₃ precipitates, *Sonderb. Prakt. Met.* 36 (2004) 125–135.
- [82] X. Hu, G. Chen, C. Ion, K. Ni, The 1100 °C isothermal section of the Ti-Ni-Si ternary system, *J. Phase Equilibria.* 20 (1999) 508–514, <http://dx.doi.org/10.1361/105497199770340761>.